

This is a repository copy of *Substrate dependent reduction of Gilbert damping in annealed Heusler alloy thin films grown on group IV semiconductors*.

White Rose Research Online URL for this paper:

<https://eprints.whiterose.ac.uk/180314/>

Version: Published Version

Article:

Love, C. J., Kuerbanjiang, B. orcid.org/0000-0001-6446-8209, Kerrigan, A. et al. (5 more authors) (2021) Substrate dependent reduction of Gilbert damping in annealed Heusler alloy thin films grown on group IV semiconductors. *Applied Physics Letters*. 172404. ISSN 0003-6951

<https://doi.org/10.1063/5.0060213>

Reuse

Items deposited in White Rose Research Online are protected by copyright, with all rights reserved unless indicated otherwise. They may be downloaded and/or printed for private study, or other acts as permitted by national copyright laws. The publisher or other rights holders may allow further reproduction and re-use of the full text version. This is indicated by the licence information on the White Rose Research Online record for the item.

Takedown

If you consider content in White Rose Research Online to be in breach of UK law, please notify us by emailing eprints@whiterose.ac.uk including the URL of the record and the reason for the withdrawal request.

Substrate dependent reduction of Gilbert damping in annealed Heusler alloy thin films grown on group IV semiconductors

Cite as: Appl. Phys. Lett. **119**, 172404 (2021); <https://doi.org/10.1063/5.0060213>

Submitted: 16 June 2021 • Accepted: 13 October 2021 • Published Online: 26 October 2021

 C. J. Love,  B. Kuerbanjiang,  A. Kerrigan, et al.



View Online



Export Citation



CrossMark

ARTICLES YOU MAY BE INTERESTED IN

[Spin wave wavevector up-conversion in Y-shaped Permalloy structures](#)

Applied Physics Letters **119**, 172403 (2021); <https://doi.org/10.1063/5.0068075>

[Ferromagnetic resonances in single-crystal yttrium iron garnet nanofilms fabricated by metal-organic decomposition](#)

Applied Physics Letters **119**, 172405 (2021); <https://doi.org/10.1063/5.0067122>

[Breaking the symmetry of spin-sublattices in antiferromagnet by interfacial tailoring in the \$\text{LiO-MnPt/NaCl/Fe}\$ junction](#)

Applied Physics Letters **119**, 172401 (2021); <https://doi.org/10.1063/5.0064931>



Timing is everything.
Now it's automatic.

A new synchronous source measure system for electrical measurements of materials and devices

 [Learn more](#)

Substrate dependent reduction of Gilbert damping in annealed Heusler alloy thin films grown on group IV semiconductors

Cite as: Appl. Phys. Lett. **119**, 172404 (2021); doi: [10.1063/5.0060213](https://doi.org/10.1063/5.0060213)

Submitted: 16 June 2021 · Accepted: 13 October 2021 ·

Published Online: 26 October 2021






View Online



Export Citation



CrossMark

C. J. Love,^{1,2}  B. Kuerbanjiang,¹  A. Kerrigan,¹  S. Yamada,³  K. Hamaya,³  G. van der Laan,²  V. K. Lazarov,¹ 
and S. A. Cavill^{1,a)} 

AFFILIATIONS

¹Department of Physics, University of York, York YO10 5DD, United Kingdom

²Diamond Light Source, Harwell Science and Innovation Campus, Didcot OX11 0DE, United Kingdom

³Center for Spintronics Research Network, Graduate School of Engineering Science, Osaka University, Osaka 560-8531, Japan

^{a)}Author to whom correspondence should be addressed: stuart.cavill@york.ac.uk

ABSTRACT

A structural and FMR study is presented for epitaxial thin films of the Heusler alloy $\text{Co}_2\text{FeAl}_{0.5}\text{Si}_{0.5}$ (CFAS) grown on Ge(111) and Si(111) substrates. All films, as-grown and post-annealed, show B2 ordering; full chemical order (L_{21}) is not obtained over the range of anneal temperatures used in this study. As-grown films show a lower Gilbert damping constant, α , when grown on a Si(111) substrate compared to Ge(111). Annealing the films to 450 °C significantly reduces α for CFAS on Ge while increasing α for CFAS on Si. This is related to a substrate dependent competition between improvements in lattice structure and increased interfacial intermixing as a function of anneal temperature. The optimal annealing temperature to minimize α is found to differ by ~ 100 K between the two substrates. Above an anneal temperature of 500 °C, films grown on both substrates have increased coercivity, decreased saturation magnetization, and show characteristic two-magnon scattering features.

Published under an exclusive license by AIP Publishing. <https://doi.org/10.1063/5.0060213>

Efficient spin-injection from ferromagnets into adjacent layers is crucial for the development of spintronic devices.¹ Spin transfer torque magnetic random access memory (STT-MRAM) based on magnetic tunnel junctions (MTJs) is seen as a frontrunner in new energy efficient nonvolatile memory. The critical current needed to switch the free layer magnetization in an STT-MRAM device is key to higher MRAM density and longevity as high write current densities can lead to failure of the tunnel barrier in the MTJ.² As the critical current density for switching is proportional to the magnetic damping and inversely proportional to the spin polarization, Heusler alloys, compounds that have the chemical formula X_2YZ with low damping and 100% spin polarization at the Fermi level, are of great interest.³ In addition, Heusler alloys are ideal for spin injection, via spin pumping, into non-magnetic materials, including technologically relevant semiconductors, such as Ge.⁴

The Heusler compounds have received much interest from a large and diverse community, partly due to the fact that the physical properties can be highly tunable exhibiting ferromagnetic,⁵ antiferromagnetic,⁶ magnetic semiconducting or even spin gapless

semiconducting behavior.⁷ The full Heusler $\text{Co}_2\text{FeAl}_{0.5}\text{Si}_{0.5}$ (CFAS) is a very promising material due to its high Curie temperature, high magnetic moment, mid-gap Fermi level, and low Gilbert damping constant, α .⁸ In addition to its thermal stability, CFAS has excellent lattice match with Ge(111) with a $\sim 0.4\%$ mismatch. On Si, the most technologically relevant substrate, the mismatch increases to 4%.⁹ One potential issue, however, is that the as-grown films tend to contain structural defects and chemical disorder, which are detrimental to the magnetic properties, such as the saturation magnetization, M_s , and α . The B2 phase, a Z/Y chemical disorder of the body center site, can be transformed to the fully order L_{21} phase by thermal annealing.¹⁰ Spin dependent density functional theory (DFT) calculations show that at the Fermi level, the L_{21} phase exhibits a finite density of states in the majority sub-band and no available states in the minority sub-band. For the B2 phase, states exist at the Fermi level for both spin sub-bands with a larger density of states in the minority sub-band, causing an opposite spin polarization compared to the L_{21} phase. This competition of opposite spin polarizations in materials with mixed phases, often found at interfaces, lowers the spin polarization. In order to

mitigate this issue, thermal annealing to transform the B2 phase to L₂₁ is, therefore, crucial, but extensive intermixing at the interface between the film and the substrate from the annealing can lead to an additional mechanism for lowering spin polarization and increased damping. Thermal annealing to improve the magnetic properties of the film may in fact result in the opposite effect.

In this paper, we present the dependence of the magnetic damping, saturation magnetization, and anisotropy of CFAS films, as measured by broadband ferromagnetic resonance, on the substrate material and post-annealing temperature. We find a reduction in the Gilbert intrinsic damping parameter, α , up to a temperature T_α . Above T_α , the FMR linewidth increases with the frequency dependence of the linewidth demonstrating enhanced intrinsic and two-magnon scattering contributions. By using a combination of x-ray diffraction and selective area electron diffraction, we show that above T_α , changes in the FMR linewidth are correlated with structural changes. T_α is found to be $\sim 450^\circ$ for CFAS on Ge(111), ~ 100 K higher than for CFAS/Si(111).

The samples were prepared by co-deposition of Co, Fe, Si, and Al using low-temperature molecular beam epitaxy. Nominally 22 nm thick CFAS films were deposited on pre-cleaned Ge (111)¹¹ and Si(111)¹² substrates at room temperature. Prior to loading substrates into the chamber, the substrate surfaces were chemically cleaned with an aqueous 1% HF solution to remove any native oxide and contamination. Annealing experiments were carried out inside a UHV chamber with a base pressure of 8×10^{-11} mbar for an hour at an indicated temperature. Structural measurements (XRD and TEM) and magnetic measurements (VSM and FMR) were performed at room temperature to characterize the films. For the FMR measurements, the sample was mounted face down onto a 50 Ω coplanar waveguide (CPW)

connected to a vector network analyzer (VNA) and centered between the poles of a 2D vector magnet. The VNA-FMR system¹³ was used for collecting angular dependent FMR spectra by measuring the microwave transmission while sweeping the microwave frequency as a function of bias field and in-plane angle.

Figure 1 shows the XRD data around the position of the (222) reflection for CFAS/Si(111). Symmetric 2θ - ω scans, which measure the out of plane momentum transfer, were used to obtain information on the (nnn) family of planes with $n = 1, 2, \text{ or } 4$. The presence of the fundamental (444) reflection, corresponding to the cubic structure (not shown), and the (222) diffraction peak is indicative of B2 ordering. The diffraction peaks were normalized to the (444) structural peaks and fitted with Voigt functions in order to extract the diffraction angle (2θ), integrated intensity (I), and linewidth (Δ_L). The Gaussian instrumental broadening was kept constant during the fitting. A lattice parameter of (5.68 ± 0.01) Å for the as-grown film is obtained from the diffraction data, consistent with that reported previously for CFAS.¹⁴ Upon annealing the integrated intensity of the (222) reflection increases with anneal temperature up to 350°C , Figs. 1(a) and 1(d), indicating improved B2 ordering. At higher anneal temperatures ($T_{\text{anneal}} > 350^\circ\text{C}$), the (222) integrated peak intensity decreases implying that the B2 ordering is progressively weakening. In addition, the diffraction angle (2θ) can be seen to move to higher angle with anneal temperature corresponding to a reduction in the lattice constant. The (111) reflection associated with the full L₂₁ chemical ordering is absent in all the films measured.

For the CFAS grown on Ge substrates, the CFAS (222) peak lies almost on top of the nominally forbidden, but still significant, (222) substrate peak because of the very small lattice mismatch between CFAS and Ge. Extracted parameters, such as integrated intensity and

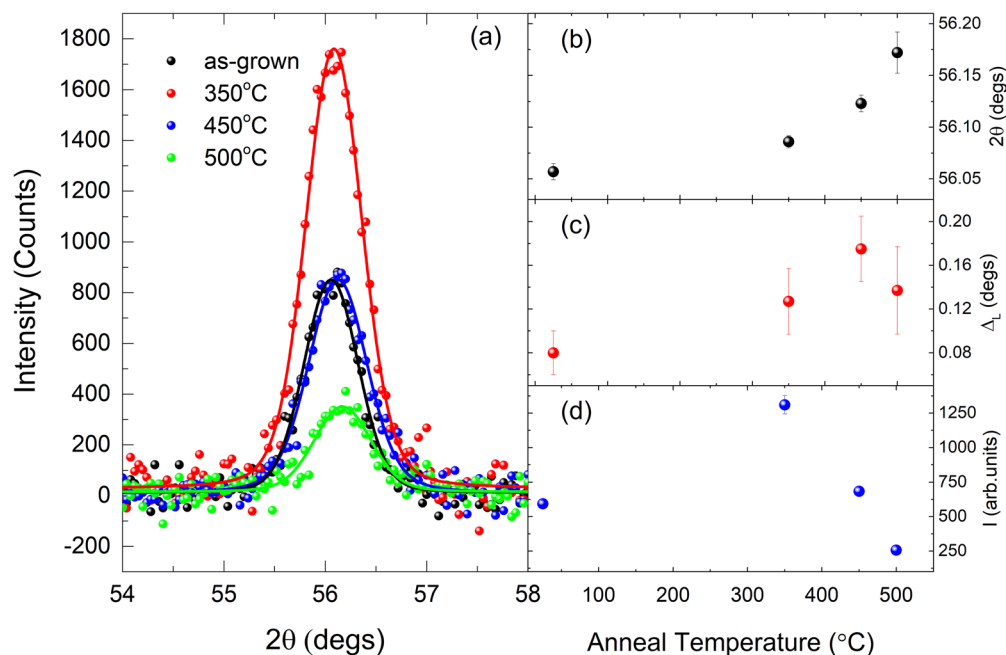


FIG. 1. (a) XRD of the CFAS/Si (111) B2 ordering peak as a function of anneal temperature. The peak position (b), Lorentzian linewidth (c), and integrated peak intensity (d) is extracted from (a) as a function of anneal temperature.

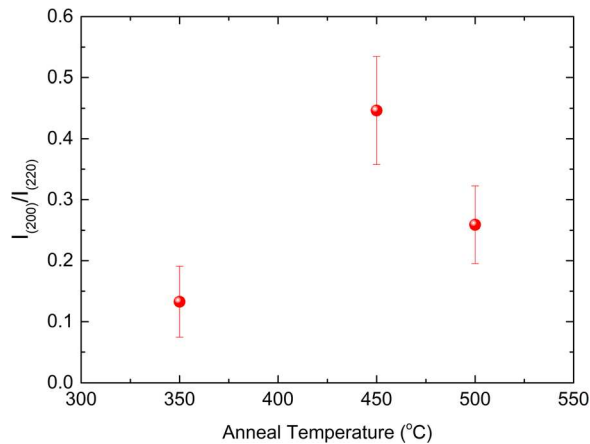


FIG. 2. Intensity ratio of the B2 ordering diffraction spot (220) to the structural diffraction spot (200) as a function of anneal temperature for CFAS/Ge(111).

diffraction angle vs anneal temperature, are difficult to obtain with reasonable error bars, and as such, we cannot comment on the temperature dependent degree of ordering from the XRD data.

To resolve this issue, we performed cross sectional electron microscopy on the films. A selective area diffraction image was recorded on each sample with the image intensity around the (200) and (220) diffraction spots integrated in order to form a ratio, which can be used as an indicator of B2 order.¹⁵ By measuring in cross

section using TEM, diffraction spots associated with the substrate are avoided. To improve the statistics, diffraction patterns from different areas of each sample were measured and averaged. Figure 2 shows the intensity of the B2 ordering (200) diffraction spot normalized to the (220) structural spot for the CFAS film.

As shown in Fig. 2, the B2 ordering is maximized at an anneal temperature of 450 °C, i.e., at 100 K higher than for CFAS on Si(111). Increasing the anneal temperature beyond this value resulted in reduced B2 ordering. The maximum of the ordering is also consistent with magnetometry data, see Fig. S1, where the saturation magnetization is maximized at $T_{\text{anneal}} = (450 \pm 10)$ °C.

Figure 3 shows XRR measurement for (a) CFAS grown on Ge and (b) CFAS grown on Si. The data were fitted using the GenX package.¹⁶ In order to improve the quality of the fit, an interface layer (between substrate and film) and a surface layer were included in the model; the interface layer accounts for intermixing between the film and substrate while the surface layer accounts for an oxidized surface as previously observed.¹⁷ The CFAS/Si and CFAS/Ge models show a reasonable agreement with the experimental XRR data. For anneal temperatures of 350 °C, both CFAS/Si and CFAS/Ge show narrow and relatively sharp interface regions. As the anneal temperature is increased, the interfacial roughness increases accordingly due to mixing,¹⁸ leading to a reduction in the amplitude of the Kiessig oscillations, especially at high angles (2θ). The XRR results are consistent with previous electron based chemical mapping, showing that, above a critical anneal temperature, intermixing between the film and the substrate is ubiquitous.¹⁸ Further details of the XRR analysis and cross-sectional TEM, showing the effect of anneal temperature on the

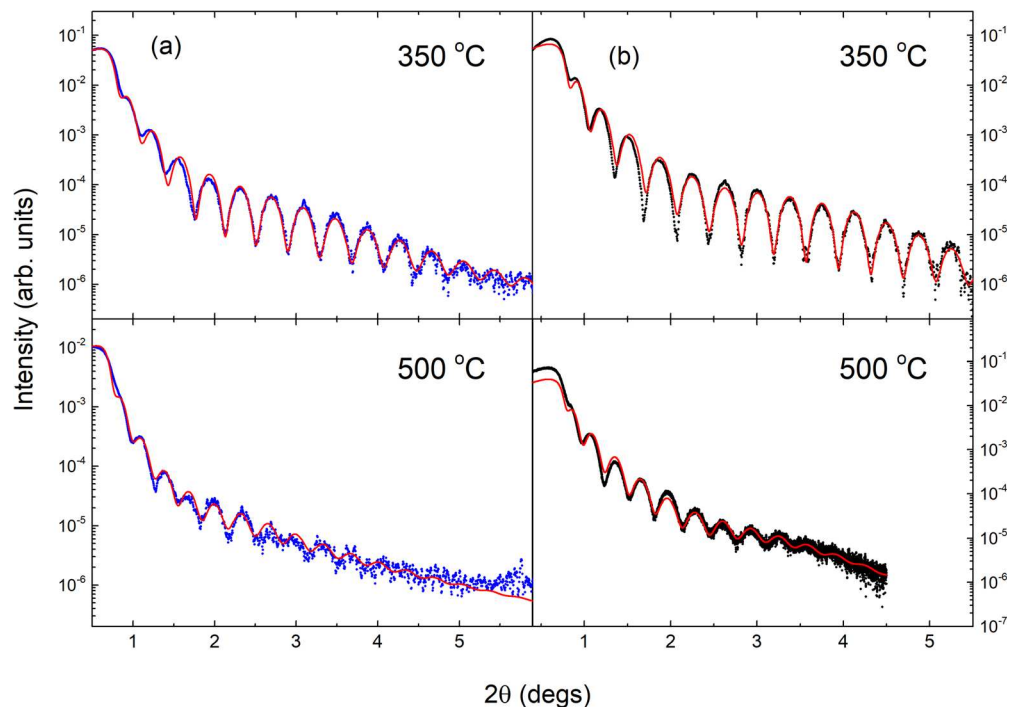


FIG. 3. (a) XRR of CFAS/Ge(111) for anneal temperatures of 300 °C (upper panel) and 500 °C (lower panel). (b) XRR of CFAS/Si(111) for anneal temperatures of 300 and 500 °C.

intermixing and size of the interface layer, can be found in the online [supplementary material](#).

In order to correlate the changes in the structure to the magnetic properties, we performed angle resolved broadband ferromagnetic resonance measurements. Figure 4 shows a 2D resonance map obtained by measuring the s-wave parameter S_{12} , which is related to the microwave transmission, as a function of frequency and applied field at $\phi = 0$ degrees (corresponding to the field applied along the $[\bar{1}0\bar{1}]$ direction).

Fits to the Kittel resonance curve along easy axis directions using

$$f = \frac{\gamma}{2\pi} \sqrt{(H + H_a)(H + H_a + 4\pi M_{\text{eff}})}, \quad (1)$$

where f is the resonant microwave frequency and H is the applied magnetic field provides values for the gyrotropic ratio, γ , anisotropy field, H_a , and the effective saturation magnetization, M_{eff} which takes into account tetragonal distortions such that

$$4\pi M_{\text{eff}} = 4\pi M_s - \frac{2K_{U\perp}}{M_s},$$

where $K_{U\perp}$ is the perpendicular anisotropy constant.

The inset in Fig. 4 shows a horizontal line scan taken through the frequency—field map at a frequency of 10 GHz, representing the field swept FMR. The data are fitted with an asymmetric Lorentzian, which is needed to account for the small mixing of the real and imaginary parts of the susceptibility,¹⁹ allowing the resonant field to be extracted as a function of azimuthal angle ϕ . For the as-grown films (Fig. 5), the in-plane anisotropy of the film is predominantly uniaxial with the easy axis along the $[\bar{1}10]$ directions. Upon annealing, the easy axis shifts toward the $[\bar{2}11]$ direction as has been observed in other Heusler films grown on (111) surfaces.²⁰ The angular plots demonstrate that an additional anisotropy is present as evidenced by the deviation away

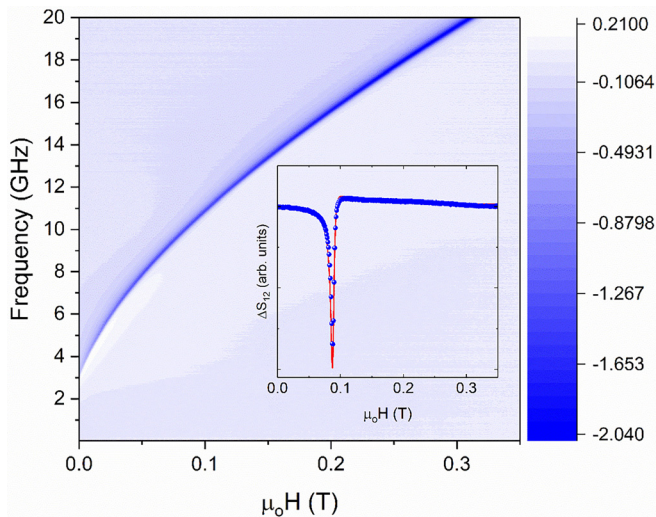


FIG. 4. Frequency—applied magnetic field map of the absorbed microwave power ΔS_{12} in dB for the magnetic field applied along the easy axis $[100]$ direction. Inset: Line scan at 10 GHz. The data (blue circles) are fitted to an asymmetric peak function (red line) allowing the linewidth, defined as the half width at half maximum, to be extracted.

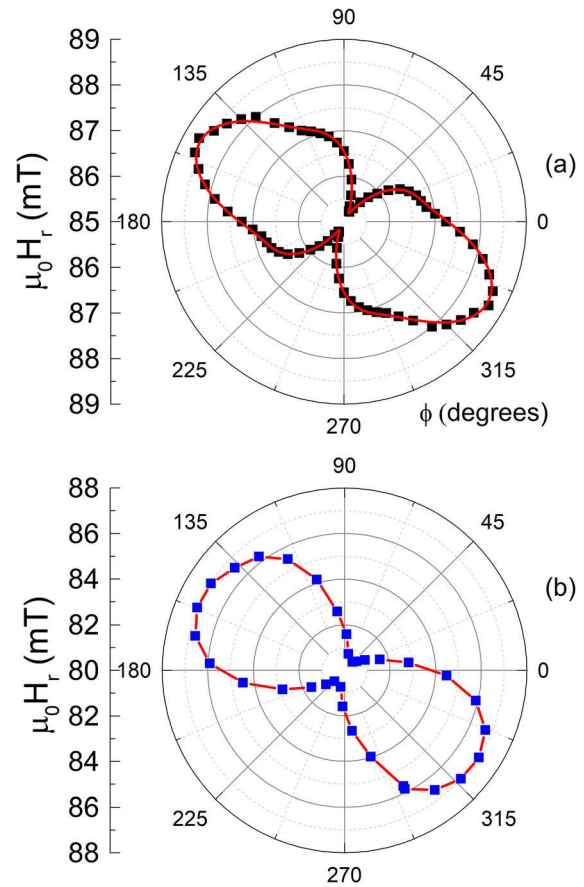


FIG. 5. Azimuthal dependence of the FMR resonance field ($\mu_0 H_r$) measured at 10 GHz for (a) CFAS/Ge and (b) CFAS/Si.

from a pure $\sin^2\phi$ dependence. For cubic magnetic thin films grown on (111) surfaces, the demagnetizing field forces the magnetic moment of the system to lie in the (111) plane. The first-order cubic magneto-crystalline anisotropy (MCA), K_c , is along the $\langle 100 \rangle$ directions for positive K_c , with the competition between the MCA and demagnetizing field resulting in a small deviation of magnetization with respect to the (111) plane. As a result, the in-plane resonance field displays sixfold symmetry with the in-plane easy axes along $\langle 110 \rangle$ for positive K_c . The cubic contribution to the measured anisotropy for a flat (111) film is very small, with variations in the resonance field on the order of 1 mT.²¹ The uniaxial magnetic anisotropy (UMA) should not be present in a pure cubic system. Uniaxial magnetic anisotropies in cubic systems are well known, particular for thin films grown on GaAs (001), and have even been observed for CFS and Fe films grown on (111) surfaces.^{22–24} For the latter systems, no adequate explanation of its origin can be found in the literature.

Growth induced anisotropy, due to the growth direction (i.e., oblique angle) or when growth takes place in a magnetic field, is often the cause of a UMA.²⁵ We can rule these effects out in our system as no magnetic field is present, and the sample is rotated during growth. Strain induced anisotropy may also lead to a UMA.¹⁹ The mismatch between Si and CFAS is 4% (Si $a = 0.543$ nm, CFAS $a = 0.568$ nm),

TABLE I. Magnetic parameters for CFAS films on Ge and Si (111) surfaces extracted from the FMR data.

Substrate	Anneal temperature (°C)	H_c (mT)	H_u (mT)	M_{eff} (emu/cc)	α ($\times 10^{-3}$)
Ge	As-grown	0.28	2.85	1025 ± 7	5.6
	350	0.24	2.21	1080 ± 7	3.8
	450	0.24	2.08	1068 ± 7	2.8
	500	0.16	1.5	1050 ± 7	...
Si	As-grown	0.26	7.2	984 ± 7	4.4
	350	0.25	5.9	1079 ± 7	4.1
	450	0.18	4.35	1041 ± 7	5.04
	500	0.40	3.4	917 ± 7	...

which would lead to a compressive biaxial strain in plane and an expansion of the lattice constant along the out of plane direction. If the strain is relaxed anisotropically, between two principle directions, a UMA could be generated by magnetoelastic coupling²⁶ to the strain. However, the symmetric 2θ - ω scans measure the lattice constant in the out of plane direction to be $(5.68 \pm 0.01)\text{\AA}$, i.e., the bulk value.¹⁴ Therefore, the strain is fully relaxed in our films. Further evidence comes from cross-sectional selective area electron diffraction from which we observe, to within error, bulk like lattice constants (along in-plane directions) for the as-grown film—see Fig. S5. The UMA is present in films grown on both substrates even though the initial mismatch is an order of magnitude larger for CFAS/Si compared to CFAS/Ge. We see no evidence of strain or anisotropic strain relaxation and believe that these effects cannot be responsible for the UMA. One possible explanation for the UMA is that step edges may lead to a preferential growth direction where the coherent domain size is larger parallel to the step edge compared to perpendicular to it, and such a hypothesis has been advocated previously.^{23,24} An anisotropy in step edge densities due to the substrate miscut generally exists. As the anneal temperature increases, leading to increased atom mobility, initial differences in the domain sizes and the UMA are reduced. Similarly to other authors, we cannot substantiate this hypothesis at this time.

A reasonable fit to the azimuthal dependence of the FMR [red line in Fig. 5(a)] is obtained by adding a cubic anisotropy term to the MCA. Uniaxial (H_u) and cubic (H_c) anisotropy fields, extracted from Fig. 5, for the films are presented in Table I. While the cubic anisotropy of the film is similar for both substrates, the UMA is significantly higher for CFAS/Si, evident from the dominant uniaxial shape of the data shown in Fig. 5(b). Reasons for this could potentially be due to differences in the step edge density between the two substrates. As the anneal temperature increases, the in-plane uniaxial anisotropy, H_u , decreases for both CFAS on Si and Ge substrates while the cubic anisotropy term is roughly constant (within error) for all but the highest anneal temperature. The increase in substrate/film intermixing with elevated anneal temperature smooths out interface effects reducing the interface induced anisotropy, consistent with the data. The cubic anisotropy, being bulk in origin, is less sensitive to interface effects. As has been noted for other intermetallic compounds grown on (111) surfaces,²⁷ a significant variation in uniaxial anisotropic features is strongly related to the interface structures.

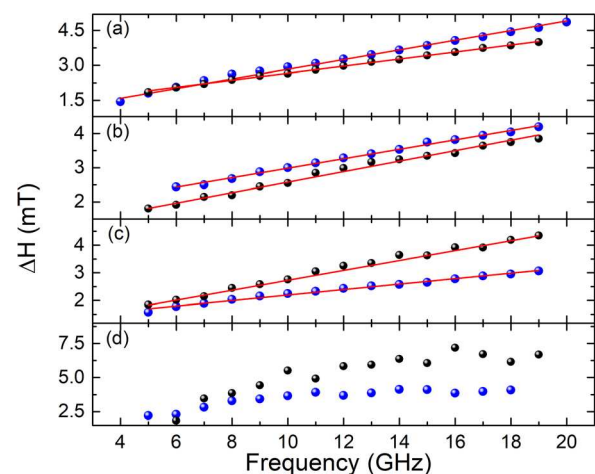
In addition to the anisotropy, FMR provides information on the Gilbert damping parameter, α , from the linearly fitted slopes of the

measured resonant field linewidth vs frequency. Figure 6 shows the resonant field linewidth dependence on frequency for the as-grown (a) and annealed samples (b)–(d). The frequency dependent linewidth, $\Delta H(f)$, which is the fitted Lorentzian HWHM, is related to the damping parameter, α , by¹⁹

$$\Delta H(f) = \Delta H(0) + \frac{2\pi\alpha f}{\gamma}, \quad (2)$$

where $\Delta H(0)$ is the frequency independent extrinsic damping. From linear fits to the plots in Fig. 6 using Eq. (2), the Gilbert damping parameter, α , is extracted as a function of anneal temperature.

For CFAS/Ge(111), α decreases for both the 350 and 450 °C annealed samples, $\alpha = 3.8 \times 10^{-3}$ and 2.8×10^{-3} , respectively, compared to the as-grown sample, $\alpha = 5.6 \times 10^{-3}$, while the extrinsic damping remains approximately constant. The sample annealed at 450 °C shows a Gilbert damping parameter 2–3 times smaller than for Permalloy²⁸ and compares well to values found in the literature for CFAS and other full Heusler films.¹⁵ At 500 °C, ΔH vs f deviates significantly from linear behavior and shows a characteristic two-magnon scattering line shape indicating magnetic inhomogeneities or mixed magnetic phases within the sample. Thus, 450 °C seems to be the optimal temperature for reducing the Gilbert damping in CFAS/

**FIG. 6.** FMR field linewidth as a function of frequency for CFAS/Ge(111) (blue) and CFAS/Si(111) (black) annealed at (a) as-grown, (b) 350, (c) 450, and (d) 500 °C.

Ge(111) and is consistent with the temperature where we observe optimal B2 ordering.

For CFAS/Si(111), the as-grown α is initially lower than for the as-grown CFAS/Ge(111). Annealing the film at 350 °C produces only a small decrease in α , unlike CFAS/Ge(111), and further temperature increases causing a significant rise in the damping constant. At $T_{\text{anneal}} = 500$ °C, the linewidth is nearly twice that of CFAS/Ge(111) above 10 GHz and again shows a characteristic two-magnon scattering line shape. Thus, for CFAS/Si(111), the optimal anneal temperature for minimizing the Gilbert damping is (100 ± 50) K lower than for CFAS/Ge(111) and again correlates with the temperature where the B2 related diffraction peak is maximized.

The reason that the optimum temperature is lower for Si substrates compared to Ge might be the slightly larger ionic radius of Ge compared to Si; Ge atoms require more energy to substitute into the CFAS lattice.

The structural and magnetic properties of the full Heusler film (CFAS) have been correlated by means of XRR/XRD and FMR. In CFAS/Si(111), the annealing strengthens the interfacial intermixing, thus enlarging the interface region and decreases the chemical ordering in the CFAS. These factors enhance the Gilbert damping, consistent with recent work.²⁹ In CFAS/Ge(111), however, the interfacial intermixing effect is not significant, even at 450 °C. The annealing process improves the lattice structure, and the Gilbert damping is decreased correspondingly. The lowest α is shown to have a direct correlation to the amount of long-range B2 ordering in the film with the optimal annealing temperature found to differ by $100 (\pm 50)$ K between Si and Ge substrates.

See the [supplementary material](#) for magnetometry data, cross-sectional TEM, and further details of the XRR analysis.

This work was partly supported by JSPS KAKENHI (Grant No. 19H05616) and EPSRC under Grant No. EP/K03278X/1.

AUTHOR DECLARATIONS

Conflict of Interest

The authors have no conflicts to disclose.

DATA AVAILABILITY

The data that support the findings of this study are available from the corresponding author upon reasonable request.

REFERENCES

- ¹B. T. Jonker, G. Kioseoglou, A. T. Hanbicki *et al.*, *Nat. Phys.* **3**, 542 (2007).
- ²B. Oliver, G. Tuttle, Q. He *et al.*, *J. Appl. Phys.* **95**, 1315 (2004).
- ³C. Guillemard, S. Petit-Watelot, L. Pasquier *et al.*, *Phys. Rev. Appl.* **11**, 064009 (2019).
- ⁴S. Kaneta –Takada, M. Yamada, S. Sato *et al.*, *Phys. Rev. Appl.* **14**, 024096 (2020).
- ⁵K. Hamaya, H. Itoh, O. Nakatsuka *et al.*, *Phys. Rev. Lett.* **102**, 137204 (2009).
- ⁶L. Scheffler, K. Gas, S. Banik *et al.*, *Phys. Rev. Mater.* **4**, 114402 (2020).
- ⁷S. Ouardi, G. H. Fecher, C. Felser, and J. Kübler, *Phys. Rev. Lett.* **110**, 100401 (2013).
- ⁸C. Banerjee, L. M. Loong, S. Srivastava *et al.*, *RSC Adv.* **6**, 77811 (2016).
- ⁹B. Kuerbanjiang, Z. Nedelkoski, D. Kepaptsoglou *et al.*, *Appl. Phys. Lett.* **108**, 172412 (2016).
- ¹⁰S. Husain, S. Akansel, A. Kumar, P. Svedlindh, and S. Chaudhary, *Sci. Rep.* **6**, 28692 (2016).
- ¹¹Y. Fujita, M. Yamada, M. Tsukahara *et al.*, *Phys. Rev. Appl.* **8**, 014007 (2017).
- ¹²S. Yamada, K. Tanikawa, S. Oki *et al.*, *Appl. Phys. Lett.* **105**, 071601 (2014).
- ¹³Rhode and Schwarz ZNB20.
- ¹⁴T. M. Nakatani, A. Rajanikanth, Z. Gercsi *et al.*, *J. Appl. Phys.* **102**, 033916 (2007).
- ¹⁵S. Mizukami, D. Watanabe, M. Oogane *et al.*, *J. Appl. Phys.* **105**, 07D306 (2009).
- ¹⁶M. Bjork and G. Andersson, *J. Appl. Crystallogr.* **40**, 1174 (2007).
- ¹⁷S. E. Glover, T. Saerbeck, B. Kuerbanjiang *et al.*, *J. Phys.: Condens. Matter* **30**, 065801 (2018).
- ¹⁸B. Kuerbanjiang, C. Love, D. Kepaptsoglou *et al.*, *J. Alloys Compd.* **748**, 323 (2018).
- ¹⁹D. E. Parkes, L. R. Shelford, P. Wadley, V. Holý, M. Wang, A. T. Hindmarch, G. van der Laan, R. P. Campion, K. W. Edmonds, S. A. Cavill, and A. W. Rushforth, *Sci. Rep.* **3**, 2220 (2013).
- ²⁰S. Yamada, K. Hamaya, K. Yamamoto *et al.*, *Appl. Phys. Lett.* **96**, 082511 (2010).
- ²¹S. M. Rezende, J. A. S. Moura, F. M. de Aугuiar *et al.*, *Phys. Rev. B* **49**, 15105 (1994).
- ²²B. K. Hazra, S. N. Kaul, S. Srinath, and M. M. Raja, *J. Phys. D: Appl. Phys.* **52**, 325002 (2019).
- ²³H.-L. Liu, W. He, Q. Wu, J. Ye, X.-Q. Zhang, H.-T. Yang, and Z.-H. Cheng, *AIP Adv.* **3**, 062101 (2013).
- ²⁴J. Ye, W. He, Q. Wu, H.-L. Liu, Z.-Y. Chen, and Z.-H. Cheng, *Sci. Rep.* **3**, 2148 (2013).
- ²⁵K. Ozawa, T. Yanada, H. Masuya *et al.* *JMMM* **35**, 289 (1983); O. Durrand, J. R. Childress, P. Galtier *et al.* *ibid.* **145**, 111 (1995).
- ²⁶O. Thomas, Q. Shen, P. Schieffer, N. Tournerie, and B. Lepine, *Phys. Rev. Lett.* **90**, 017205 (2003).
- ²⁷Y. Ando, K. Hamaya, K. Kasahara *et al.*, *J. Appl. Phys.* **105**, 07B102 (2009).
- ²⁸Y. Zhao, Q. Song, S.-H. Yang *et al.*, *Sci. Rep.* **6**, 22890 (2016).
- ²⁹Q. Gao, X. Lu, Z. Chen *et al.*, *Appl. Phys. Lett.* **116**, 212406 (2020).